KSCE Journal of Civil Engineering (2019) 23(9):4141-4153

DOI 10.1007/s12205-019-0068-4

Tunnel Engineering

pISSN 1226-7988, eISSN 1976-3808
www.springer.com/12205

Complex Analysis of Ground Deformation and Stress for a Shallow Circular Tunnel with a Cavern in the Strata considering the Gravity Condition

Gongbiao Yang*, Chengping Zhang, Yi Cai***, and Bo Min******

Received January 11, 2019/Revised April 20, 2019/Accepted June 25, 2019/Published Online August 6, 2019

Abstract

In the urban strata, the caverns appear inevitably due to the leakage of pipelines, the constructions of underground structures and other factors. For shallow tunnels, the influences of caverns on the ground deformation and stress during the tunneling construction cannot be ignored, which may endangers the surrounding understructures and nearby superstructures. Therefore, the interaction between the tunnel and the cavern should be considered seriously. In order to achieve ground deformation and stress for a shallow circular tunnel with a cavern in the strata, an analytical model that can take into account the gravity and the interaction between the tunnel and the cavern is proposed in this paper. In the model, the initial gravity condition is considered on the tunnel boundary, and the stress free condition is taken into account on the cavern boundary. During the solving process, the complex variable method and the Schwarz alternating method are applied. Then the analytical solution is verified by a corresponding numerical model. The results show that the analytical solution for the deformation and stress on the tunnel boundary agrees very well with the numerical solution. Finally, the influences of the cavern on the hoop stresses, radial deformations along the tunnel boundary and the surface settlements are discussed based on the solution proposed. The research shows important theoretical significances and application potentials for the prediction of the ground stress and deformation caused by the shallow tunnel with a cavity in the stratum.

Keywords: *complex variables, Schwarz alternating method, shallow tunnel, cavern, stress and displacement*

1. Introduction

As the development of underground transportation, the constructions of urban tunnels are increased dramatically. In the urban strata, the caverns appear inevitably due to the leakage of pipelines, the constructions of underground structures and other factors. Generally, the depths of the tunnels in urban area are relatively shallow, which are greatly affected by the underground caverns and other geological diseases. Therefore, it is of great significance for the safety of nearby understructures and superstructures to assess accurately the ground stress and deformation induced by the shallow tunnel with a cavern in the strata.

For shallow tunnels, researchers and engineers have performed many investigations for the displacement induced by tunneling excavation owing to its influence on the safety of tunnel itself and nearby structures. Based on a large of investigations, the Gaussian function was initially proposed by Peck (1969) to predict surface settlement. In practice, this method was widely used by researchers due to its convenience and simplicity. However, the empirical formula cannot reveal the internal mechanism of ground deformation, which limits its further development. Sagaseta (1987) proposed the virtual image methodology that reduced the deformation at the tunnel boundary to the volume loss at the tunnel center. By using this method, some solutions of the stress and displacement field were presented (Verruijt and Booker, 1996; Zhang *et al*., 2019) with considering the more complicated deformation pattern on the tunnel boundary. The "equivalent ground loss parameter" was put forward by Lee *et al*. (1992) for assessing the ground displacement in soft clays, which could take into account the physical gap (the space between the lining and the external outline of the shield), the workmanship quality and equivalent 3D elastic-plastic deformation at the tunnel surface. Moreover, a semi-analytical solution of ground deformation was obtained (Loganathan and Poulos, 1998) by use of the closed-form solution put forward by Verruijt and Booker (1996) and the "equivalent ground loss parameter". Bobet (2001) presented elastic solutions of ground deformation

*Ph.D. Candidate, Key Laboratory of Urban Underground Engineering of Ministry of Education, Beijing Jiaotong University, Beijing 100044, China (E-mail: 16115278@bjtu.edu.cn)
**Professor, Key Laboratory of Urban Underground Engineering of Ministry of Education, Beijing Jiaotong University, Beijing 100044, China (Corresponding Author, E-mail: chpzhang@bjtu.edu.cn)
***Ph.D. Candidate, Key Laboratory of Urban Underground Engineering of Ministry of Education, Beijing Jiaotong University, Beijing 100044, China (E-mail: 13115295@bjtu.edu.cn)
****Ph.D. Candidate, Key Laboratory of Urban Underground Engineering of Ministry of Education, Beijing Jiaotong University, Beijing 100044, China (E-mail: 16115288@bjtu.edu.cn)

for a shallow tunnel by expanding the stress function method. However the non-uniform deformation pattern on the tunnel boundary weren't considered in the solution. Park (2004) proposed four typical deformation models (including uniform radial deformation, oval deformation and vertical settlement) on the tunnel boundary, and the solutions for each model were obtained by using stress function method. Considering the above non-uniform convergence pattern between the liner and the ground, Zhang *et al*. (2017) proposed a closed-form analytical solution of liner internal forces and surrounding soil deformation caused by shallow tunnels. However, these theories are not suitable for studying the interaction between the tunnel and the cavern.

Since a long time, the development of the complex variable theory has provided a new way to solve the elastic problems, especially for the problems in rock engineering. By application of the conformal mapping method, Verruijt (1997, 1998) proposed a new method for a shallow tunnel in the semi-infinite plane without taking into account the body force. Then, the complex variable solutions of the tunnel with uniform displacement on its boundary (Verruijt, 1997) and uniform radial stress on its boundary (Verruijt, 1998) were presented successively. Combining with Schwarz method, Fu *et al*. (2015) presented a complex variable solution of twin-parallel shallow tunnels with uniform deformation on their outlines. A complex variable solution, with taking account of the interaction mechanism between the ground and liners, for predicting ground displacement and liner internal force of shallow tunnels was presented by Zhang *et al*. (2018). However, the gravity effect was not involved for the above solutions. There will be an inaccurate evaluation in the results without considering gravity, because the significant impact of body force on the shallow tunnels. In order to consider the effect of gravity, a logarithm term was added in the complex potential function by Strack and Verruijt (2002), and an analytical solution was proposed for a shallow tunnel with deforming boundary conditions. Nevertheless, the distribution of the unbalanced force on the outline of the tunnel was not considered. After that, Lu *et al*. (2016) proposed a complex variable solution for a shallow circular tunnel by considering the detailed distribution of gravity on the tunnel boundary.

With the development of computer technology, numerical simulations were widely used in tunnel engineering. Lee *et al*. (1990) studied the ground deformation during the excavation of a shield tunnel in soft layer through finite element analysis. Migliazza *et al*. (2009) simulated the excavation and supporting process of the tunnel by use of a 3D finite element model, and compared the ground settlements with the field monitoring results. Moreover, the numerical method was applied for investigating the ground subsidence caused by the excavation of twin tunnels and the interactions between them (Addenbrooke and Potts, 2001; Do, *et al*., 2016). In addition, there are a variety of construction methods in practice and the optimization of construction methods are conducted numerically. By use of numerical method, the internal force of the structure and the ground subsidence during the construction of PBA (pile-beam-arch) subway station, which has been widely used in the subway stations in China, were studied by Liu *et al*. (2017). Zhou *et al*. (2018, 2019) presented a phase field model for simulating complex fracture patterns in rock by developing the professional commercial software COMSOL Multiphysics.

So far, the problem of strata cavities has attracted the attentions of relevant scholars. Goodings and Abdulla (2002) studied the development of sinkholes in arid areas with karst bed rock through the centrifuge model test. Based on the bound theorems of classical plasticity, Augarde *et al*. (2003) performed a novel numerical simulation to predict the collapse of a submerged spherical cavity. According to the investigation of Beijing metro line 4 and line 10, Fang *et al*. (2011) found that strata caverns frequently happened to the construction of tunnels, and the accidents induced by caverns have caused heavy property losses and casualties. An analytical solution for a cavern with different shapes was proposed by use of the complex variable method, and the initial distribution of plastic zone around the cavern was obtained based on Mohr-Coulomb failure criterion (Li *et al.*, 2014). However, the interaction between the cavern and the tunnel is not considered in this solution. By conducting a series of model tests, Zhang *et al*. (2016) study the influence of the position and quantity of hidden caverns on the ground damage during the tunneling construction.

In summary, there are few theoretical studies about the interaction between the cavern and the shallow tunnel during construction, and the gravity factor is rarely considered. However, the interaction may influence the ground stress and deformation, which subsequently endangers the underground structures and superstructures. Moreover, the gravity is the main external load for shallow tunnels, so it is not suitable to ignore its influence in the solution process. In this paper, an analytical model is established for a shallow tunnel with a cavern in the strata, which could take into account the gravity effect and the interaction between the tunnel and the cavern. Then, the analytical solution is presented for the model by using of complex variable method and Schwarz alternating method. Finally, the effects of the cavern on the tunnel and surface settlements are investigated based on the analytical solution.

2. Analytical Model and Solving Methods

2.1 Analytical Model

The excavation of a shallow circular tunnel with a cavern in the strata is simplified as a model in the Z half-plane (Fig. 1). The plane-strain assumption is adopted in the following derivation. The Z half-plane includes the Z_1 half-plane and the Z_2 half-plane, which are corresponded to the coordinate system $x_1o_1y_1$ and the coordinate system $x_2o_2y_2$, respectively. The distance between the origins of the two coordinate systems is c, and the distance between the centers of the two cavities is d. The radius and center depth of the tunnel are r_1 and h_1, and those of the cavern are r_2 and h_2.

The displacement caused by the cavern has been completed

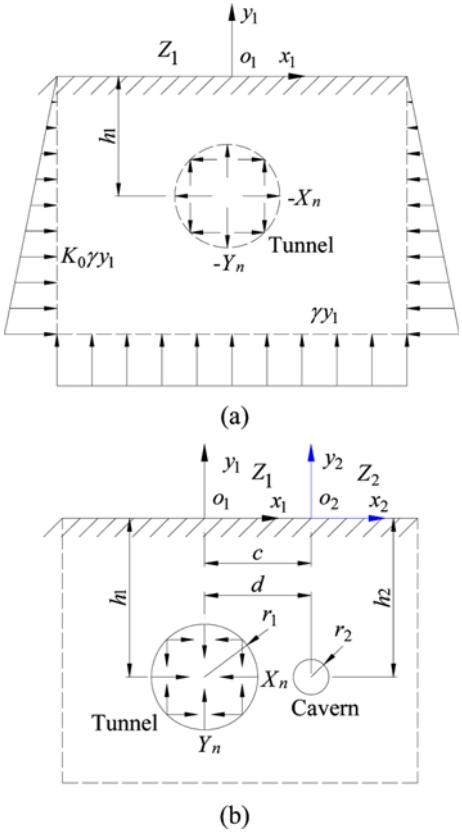

Fig. 1. Simplified Analytical Model of a Shallow Circular Tunnel with a Cavern in the Strata: (a) Tunnel Unexcavated, (b) Tunnel Excavated

before the tunnel excavation, so this part of displacement is ignored during the tunnel construction. Generally, the caverns are smaller than tunnels, and the stresses caused by the caverns have been redistributed gradually over time. Therefore, the stresses on the tunnel boundary before excavation are still dominated by initial gravitational field. The excavation of a tunnel is equivalent to relieving the original surface force along its boundary, that is, imposing the equal but opposite force on its boundary. So, it is assumed that the force imposed along the tunnel boundary in Fig. 1(b) is equal to the stress as shown in the Fig. 1(a), but their directions are opposite. Furthermore, both of the cavern boundary and the surface boundary are free of stress.

2.2 Solving Method

The Schwarz alternating method divides the problem of a multiply-connected region into a series of problems of single-connected regions, and every problem of a single-connected region could be solved easily. Then the solution for the problem of a multiply-connected region can be obtained by the superposition of these solutions of single-connected regions.

The complex variable method and the Schwarz alternating method are applied to solve the problem shown in Fig. 1. The tunnel is represented by 1 and the cavern is represented by 2 in the following discussion. Taking the first iteration process as an example, the solution process is as follows.

1. Assuming that there is only a shallow circular tunnel in the Z_1 half-plane, the reverse initial gravity stress is imposed on the tunnel boundary, then the analytic functions $\varphi_{11}(z_1)$ and $\psi_{11}(z_1)$ could be obtained by use of the complex variable method. Consequently, the stress and displacement caused by the tunnel in the Z_1 half-plane can be deduced.
2. The tunnel excavation results in the stresses on the cavern boundary. In order to keep the cavern boundary is free of stress, these stresses need to be applied in opposite directions on the cavern boundary (named additional surface force). By coordinate transformation, the additional surface force $f_{11}(\alpha_2\sigma_2)$ could be determined by $\varphi_{11}(z_1)$ and $\psi_{11}(z_1)$ in terms of series.
3. Assuming that there is only a cavern in Z_2 half-plane, and $f_{11}(\alpha_2\sigma_2)$ is imposed on the cavern boundary, analytic functions $\varphi_{21}(z_2)$ and $\psi_{21}(z_2)$ could also be obtained by use of the complex variable method.
4. The cavern will lead to stresses on the tunnel boundary again, which also need to be imposed on tunnel boundary in opposite directions. By coordinate transformation, the additional surface force $f_{21}(\alpha_1\sigma_1)$ could also be determined by $\varphi_{21}(z_2)$ and $\psi_{21}(z_2)$ in terms of series.

The first subscript of φ, ψ and f indicates the serial number of the cavity, while the second subscript of them indicates the number of iterations. Both of the tunnel and the cavern are each imposed additional surface force is an entire iteration. It should be worth noting that the surface traction imposed on the tunnel boundary in the first iteration is the equal but opposite to the initial gravity stress, but not additional surface force. The process of subsequent iterations is same as the first iteration except that the reverse initial gravity stress is replaced by the additional surface force on the tunnel boundary. The repetitive process should be conducted until both of the additional force on the cavern boundary and the tunnel boundary are trend to zero with a proper accuracy. With the increase of the iterations, the additional surface force will be decreased. Owing to the limitation of Schwarz alternating method, it is impossible that the additional surface forces on the tunnel boundary and the cavern boundary are equal to zero simultaneously. As long as the number of iterations is sufficient, the solution is accurate enough for engineering applications. Subsequently, the final result can be obtained by the superposition of all the iterations.

2.3 Assumptions

In order to solve the problem more conveniently, some assumptions are made in the solving process as follows.

1. The problem is solved under the plane-strain condition.
2. It is assume that the stratum is a semi-infinite homogeneous elastic plane, which conforms to the Hooke's law.
3. The initial gravity boundary condition is considered on the tunnel boundary
4. The ground is assumed to conform to small deformation hypothesis, so the changes of shape and position of the tunnel and the cavern are neglected during the iterative process.

3. Solving Process

3.1 The First Solution for the Tunnel

Under the actions of X_n and Y_n along the tunnel boundary (shown in the model Fig. 1(b)) in the semi-infinite plane without the cavern, the complex potential analytic functions $\psi_{11}(z_1)$ and $\psi_{11}(z_1)$ in Z_1 half-plane can be expressed in the following forms

$$\varphi_{11}(z_1)=-\frac{F_{1x}+iF_{1y}}{2\pi(1+\kappa)}\left[\kappa\ln\left(z_1-\overline{z_{1c}}\right)+\ln\left(z_1-z_{1c}\right)\right]+\varphi_0(z_1) \tag{1}$$

$$\psi_{11}(z_1)=\frac{F_{1x}-iF_{1y}}{2\pi(1+\kappa)}\left[\ln\left(z_1-\overline{z_{1c}}\right)+\kappa\ln\left(z_1-z_{1c}\right)\right]+\psi_0(z_1) \tag{2}$$

where $z_1=x_1+iy_1$. κ is a material constant determined by Poisson's ratio μ, $\kappa=3-4\mu$ under plane-strain condition. $z_{1c}=-ia_1$, a_1 can be determined by the conformal mapping function. $\varphi_0(z_1)$ and $\psi_0(z_1)$ are single-valued analytic functions, which can be expressed by Laurent series. $F_{1x}=\oint X_n ds=0$, $F_{1y}=\oint Y_n ds=\pi r_1^2\gamma$ where γ is uniform volumetric weight, X_n and Y_n are surface traction components on the tunnel boundary in x_1 and y_1 direction, respectively.

The analytic functions $\varphi_{11}(z_1)$ and $\psi_{11}(z_1)$ can be determined based on the following boundary conditions. The stress boundary condition can be expressed by the equation

$$\varphi_{11}(z_1)+z_1\overline{\varphi'_{11}(z_1)}+\overline{\psi_{11}(z_1)}=i\int_A^B(X_n+iY_n)ds+C_1 \tag{3}$$

where z_1 indicates a point at the tunnel boundary. Point A and point B (shown in Fig. 2) denote the starting point and ending point of the integral path, respectively. The region studied should be on the left side of the integral path when integrating from point A to point B. C_1 is an integral constant. Without loss of generality, $C_1=0$ is considered on one of the boundaries, but C_1 is an unknown value to be determined on other boundaries.

On the surface boundary ($y_1=0$), $X_n=0$, $Y_n=0$. With Eq. (3), the boundary condition can be expressed by

$$\varphi_{11}(z_1)+z_1\overline{\varphi'_{11}(z_1)}+\overline{\psi_{11}(z_1)}=0 \tag{4}$$

Before excavating, the stresses in the lower half-plane ($y_1<0$) are

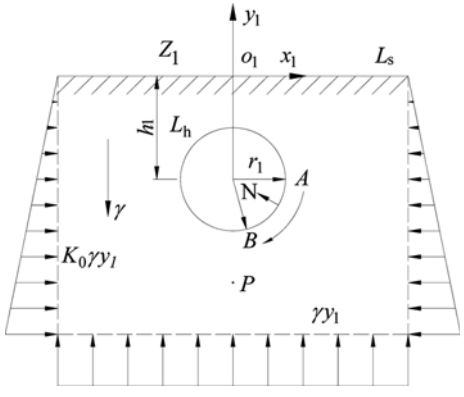

Fig. 2. Shallow Circular Tunnel under Gravity Condition

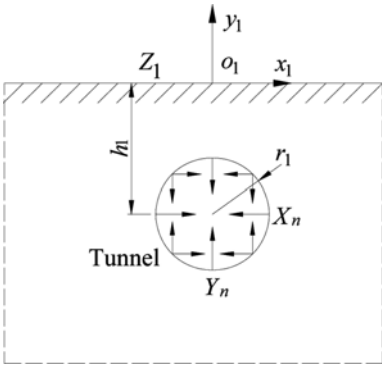

Fig. 3. Equal and Opposite Forces around the Tunnel Boundary

$$\begin{cases}\sigma_y^0=\gamma y_1\\ \sigma_x^0=K_0\sigma_y^0\\ \tau_{xy}^0=0\end{cases} \tag{5}$$

where K_0 is the lateral pressure coefficient. The excavation of a tunnel is considered by applying the equal but opposite surface traction along its boundary (shown in Fig. 3). According to the static equilibrium relationship, surface traction on the boundary can be expressed

$$\begin{cases}X_n ds=-\left(\sigma_x^0 l ds+\tau_{xy}^0 n ds\right)\\ Y_n ds=-\left(\sigma_y^0 n ds+\tau_{xy}^0 l ds\right)\end{cases} \tag{6}$$

where l and n denote the cosines of the outward normal unit vector in x_1 and y_1 direction on the tunnel boundary, respectively.

$$\begin{cases}l=\cos\left(\mathrm{N},x_1\right)=\dfrac{dy_1}{ds}\\ n=\cos\left(\mathrm{N},y_1\right)=-\dfrac{dx_1}{ds}\end{cases} \tag{7}$$

By substituting Eqs. (5) – (7) into Eq. (3), then it can be expressed as

$$\varphi_{11}(z_1)+z_1\overline{\varphi'_{11}(z_1)}+\overline{\psi_{11}(z_1)}=-iK_0\int_A^B y_1dy_1-\gamma\int_A^B y_1dx_1+C_1 \tag{8}$$

As shown in Fig. 4, the Z_1 half-plane is mapped conformally into an annular region in the ζ_1-plane that are bounded by the outer circle $|\zeta_1|=1$ and the inner circle $|\zeta_1|=\alpha_1$, where $\alpha_1<1$. With the conformal transformation in Eq. (9), the outer circle $|\zeta_1|=1$ is corresponded to the ground surface, and the inner circle $|\zeta_1|=\alpha_1$ is corresponded to the tunnel boundary.

$$z_1=\omega_1(\zeta_1)=-ia_1\frac{1+\zeta_1}{1-\zeta_1} \tag{9}$$

where $a_1=h_1(1-\alpha_1^2)/(1+\alpha_1^2)$, and α_1 is a parameter determined by $r_1/h_1=2\alpha_1/(1+\alpha_1^2)$.

After the conformal mapping, $\varphi_0(z_1)$ and $\psi_0(z_1)$ can be expressed as functions of ζ_1, which are denoted by $\varphi_0(\zeta_1)$ and $\psi_0(\zeta_1)$, respectively. They can further be expanded by the Laurent series

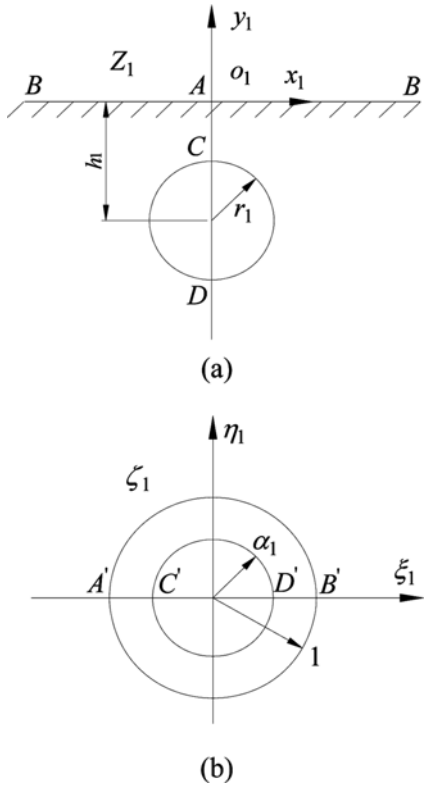

Fig. 4. Conformal Transformation of Z_1 Half-plane to ζ_1-plane: (a) Z_1 Half-plane, (b) ζ_1-plane

$$\varphi_0(\zeta_1)=\sum_{k=0}^{\infty}a_k^{11}\zeta_1^k+\sum_{k=1}^{\infty}b_k^{11}\zeta_1^{-k} \tag{10}$$

$$\psi_0(\zeta_1)=\sum_{k=0}^{\infty}c_k^{11}\zeta_1^k+\sum_{k=1}^{\infty}d_k^{11}\zeta_1^{-k} \tag{11}$$

where the coefficients $a_k^{11}, b_k^{11}, c_k^{11}$ and d_k^{11} will be determined according to boundary conditions. The first superscript of these coefficients indicates the serial number of the cavity, while the second superscript of them indicates the number of iterations.

Substituting Eqs. (1), (2), (9), (10) and (11) into Eq. (4), the boundary condition of the ground surface ($\zeta_1=\sigma=e^{i\theta}$) is represented as

$$\varphi_0(\sigma)+\frac{1}{2}\left(1-\sigma^{-2}\right)\overline{\varphi_0'(\sigma)}+\overline{\psi_0(\sigma)}=\sum_{k=-\infty}^{+\infty}A_k\sigma^k \tag{12}$$

where

$$\begin{cases}A_0=-\dfrac{i\gamma r_1^2}{4}\\ A_1=-\dfrac{i\gamma r_1^2}{4(1+\kappa)}\\ A_{-1}=-\dfrac{i\kappa\gamma r_1^2}{4(1+\kappa)}\\ A_k=0,\ \ (k=\pm2,\pm3,\cdots)\end{cases} \tag{13}$$

Substituting Eqs. (10) and (11) into Eq. (12), then the following relationships are obtained by setting all the power coefficients equal to zero.

$$\begin{cases}c_0^{11}=\overline{A_0}-\overline{a_0^{11}}-\dfrac{1}{2}a_1^{11}-\dfrac{1}{2}b_1^{11}\\ c_k^{11}=\overline{A_{-k}}-\overline{b_k^{11}}+\dfrac{1}{2}(k-1)a_{k-1}^{11}-\dfrac{1}{2}(k+1)a_{k+1}^{11},\ \ (k\ge1)\\ d_k^{11}=\overline{A_k}-\overline{a_k^{11}}+\dfrac{1}{2}(k-1)b_{k-1}^{11}-\dfrac{1}{2}(k+1)b_{k+1}^{11},\ \ (k\ge1)\end{cases} \tag{14}$$

Equation (14) shows the coefficient relationships of the two analytic functions. If the coefficients a_k^{11} and b_k^{11} can be found, the coefficients c_k^{11} and d_k^{11} would be determined by Eq. (14). It is not yet enough to determine all the coefficients, therefor some additional boundary conditions are required to determine the remaining unknown coefficients a_k and b_k.

On the tunnel boundary ($\zeta_1=\alpha_1\sigma$), Eq. (9) gives

$$x_1=\frac{z_1+\overline{z_1}}{2}=-i\frac{a_1}{2}\left(\frac{1+\alpha_1\sigma}{1-\alpha_1\sigma}-\frac{\sigma+\alpha_1}{\sigma-\alpha_1}\right) \tag{15}$$

$$y_1=\frac{z_1-\overline{z_1}}{2}=-\frac{a_1}{2}\left(\frac{1+\alpha_1\sigma}{1-\alpha_1\sigma}+\frac{\sigma+\alpha_1}{\sigma-\alpha_1}\right) \tag{16}$$

Substituting Eqs. (1), (2), (15) and (16) into Eq. (8), then the condition on the tunnel boundary is represented as

$$\begin{aligned}&(1-\alpha_1\sigma)\left[\varphi_0(\alpha_1\sigma)+\frac{\omega_1(\alpha_1\sigma)}{\overline{\omega_1'(\alpha_1\sigma)}}\overline{\varphi_0'(\alpha_1\sigma)}+\overline{\psi_0(\alpha_1\sigma)}\right]\\ &\quad=\sum_{k=-\infty}^{\infty}B_k\sigma^k+C_1(1-\alpha_1\sigma)\end{aligned} \tag{17}$$

where B_k is shown in Appendix 1.

Substituting Eqs. (10), (11) and (14) into Eq. (17), then the following relationships are obtained by setting all the power coefficients equal to zero.

$$\sigma^0:\left(1-\alpha_1^2\right)a_1^{11}+\left(1-\alpha_1^2\right)\overline{b_1^{11}}=-\overline{B_0}-\overline{C_1}+\overline{A_0}-\overline{A_{-1}}\alpha_1^2 \tag{18}$$

$$\sigma^1:\left(1-\alpha_1^2\right)a_1^{11}+\left(1-\alpha_1^2\right)\overline{b_1^{11}}=-B_1\alpha_1+C_1\alpha_1^2-A_0\alpha_1^2+A_1 \tag{19}$$

$$\begin{aligned}\sigma^{k+1}:&\left(\alpha_1^{-k+1}-\alpha_1^{k+1}\right)a_k^{11}+k\left(\alpha_1^{-k-1}-\alpha_1^{-k+1}\right)\overline{b_k^{11}}+\left(\alpha_1^{k+1}-\alpha_1^{-k-1}\right)a_{k+1}^{11}\\ &+(k+1)\left(\alpha_1^{-k+1}-\alpha_1^{-k-1}\right)\overline{b_{k+1}^{11}}=B_{k+1}+A_k\alpha_1^{-k+1}-A_{k+1}\alpha_1^{-k-1},\ \ (k\ge1)\end{aligned} \tag{20}$$

$$\begin{aligned}\sigma^{-k}:&k\left(\alpha_1^k-\alpha_1^{k+2}\right)a_k^{11}+\left(\alpha_1^{-k}-\alpha_1^k\right)\overline{b_k^{11}}+(k+1)\left(\alpha_1^{k+2}-\alpha_1^k\right)a_{k+1}^{11}\\ &+\left(\alpha_1^{k+2}-\alpha_1^{-k}\right)\overline{b_{k+1}^{11}}=\overline{B_{-k}}-\overline{A_{-k}}\alpha_1^k+\overline{A_{-k-1}}\alpha_1^{k+2},\ \ (k\ge1)\end{aligned} \tag{21}$$

It follows from Eqs. (18) and (19) that

$$\overline{C_1}+C_1\alpha_1^2=\overline{A_0}-\overline{B_0}-A_1+B_1\alpha_1+\left(A_0-\overline{A_{-1}}\right)\alpha_1^2 \tag{22}$$

The constant C_1 can be determined by Eq. (22).

Equations contained in Eqs. (20) and (21) are infinite, but k cannot be an infinite value in actual solutions. It is assumed that the number of non-zero positive and negative terms contained in $\varphi_0(\zeta_1)$ is N, that is, a_k and b_k are equal to zero while $k>N$. Due to the convergence of the series $\varphi_0(\zeta_1)$ and $\psi_0(\zeta_1)$, the solution becomes more accurate with the increase of N. The value of k is taken from 1 to $N-1$ in Eq. (20) and from 1 to N in Eq. (21), and an equation is taken from Eq. (18) or Eq. (19). There are $2N$ equations for $2N$ coefficients, so the coefficients can be determined entirely by these equations. Then, c_k and d_k (k = 1, 2, ..., N + 1) can be determined by Eq. (14).

The coefficient a_0 represents the rigid body displacements of the half-plane, which does not affect the stresses and can be determined by fixing a point, like the point P in Fig. 1. Then the coefficient c_0^{11} can be given by Eq. (14).

3.2 The Additional Surface Force on the Cavern Boundary

Zhang *et al*. (2000) proposed a method to determine the additional surface force by coordinate transformation. According to this method, Yan *et al*. (2011) obtained the approximation of the additional surface force by Fourier series. This method just needs to transform the coordinates of points on cavern boundary instead of transforming the two analytic functions, which can be carried out easily by a computer script. The expression of the additional surface force on the cavern boundary caused by the tunnel can be written as follows

$$-f_{11}(\alpha_2\sigma)=\varphi_{11}(\eta_1)+\frac{\omega_1(\eta_1)}{\overline{\omega_1'(\eta_1)}}\overline{\varphi_{11}'(\eta_1)}+\overline{\psi_{11}(\eta_1)} \tag{23}$$

The negative sign on the left side of Eq. (23) indicates that the surface forces caused by the tunnel excavation are applied in the opposite directions on the cavern boundary. The main procedures are shown as follows. 1) Coordinate of the point $\eta_2=\alpha_2\sigma$ on the cavern boundary in ζ_2 plane is taken. 2) By conformal mapping $t_2=\omega_2(\eta_2)$, coordinate of the point in Z_2 half-plane is obtained. 3) By coordinate transformation $t_1=t_2+c$, coordinate of the point in Z_1 half-plane is obtained. 4) By inverse conformal mapping $\eta_1=\omega_1^{-1}(t_1)$, coordinate of the point in ζ_1 plane is obtained. 5) Substituting η_1 in Eq. (23), the additional surface forces on the cavern boundary in the ζ_2 plane are obtained.

In order to improve the solving efficiency, the additional surface force is represented by a series

$$f_{11}(\eta_2)=\sum_{k=-m}^{m}E_k\sigma^k \tag{24}$$

The accuracy of the approximation for the additional surface force in Eq. (24) is higher with larger value of m. The points on the cavern boundary can be expressed in polar coordinates, i.e. $\eta_2=\alpha_2\sigma=\alpha_2 e^{i\theta}$. The additional surface force can also be rewritten as a function of θ

$$f_{11}(\theta)=g_1(\theta)+ig_2(\theta) \tag{25}$$

where $g_1(\theta)$ and $g_2(\theta)$ are the real part and the imaginary part of $f_{11}(\theta)$, respectively. Both of them are real functions in the interval $0\le\theta\le2\pi$. Then $g_1(\theta)$ can be expressed as a trigonometric series

$$g_1(\theta)=\frac{1}{2}\lambda_0+\sum_{k=1}^{m}(\lambda_k\cos k\theta+\delta_k\sin k\theta) \tag{26}$$

Obviously, $g_1(\theta)$ has a periodic of 2π. M points are taken equidistantly in the interval $(0, 2\pi)$

$$\theta_j=\frac{2\pi}{M}j,(j=0,1,\cdots,M-1) \tag{27}$$

According to the orthogonality of trigonometric function, the coefficients in Eq. (24) can be obtained

$$\begin{cases}\lambda_0=\dfrac{2}{M}\displaystyle\sum_{j=0}^{M-1}g_1(\theta_j)\\ \lambda_k=\dfrac{2}{M}\displaystyle\sum_{j=0}^{M-1}g_1(\theta_j)\cos(k\theta_j),\ (k=1,2,\cdots,m)\\ \delta_k=\dfrac{2}{M}\displaystyle\sum_{j=0}^{M-1}g_1(\theta_j)\sin(k\theta_j),\ (k=1,2,\cdots,m)\end{cases} \tag{28}$$

$g_2(\theta)$ can also be expressed as a trigonometric series with the corresponding coefficients λ_0', λ_k' and δ_k'. With $\cos(k\theta)=(e^{ik\theta}+e^{-ik\theta})/2=(\sigma^k+\sigma^{-k})/2$ and $\sin(k\theta)=(e^{ik\theta}-e^{-ik\theta})/2=(\sigma^k-\sigma^{-k})/2$, Eq. (24) can be expressed as

$$f_{11}(\gamma_2)=f_{11}(\theta)=\sum_{k=-m}^{m}E_k\sigma^k \tag{29}$$

where

$$\begin{cases}E_0=(\lambda_0+i\lambda_0')/2\\ E_k=\left[(\lambda_k+\delta_k')+i(\lambda_k'-\delta_k)\right]/2,\ (k=1,2,\cdots,m)\\ E_{-k}=\left[(\lambda_k-\delta_k')+i(\lambda_k'+\delta_k)\right]/2,\ (k=1,2,\cdots,m)\end{cases} \tag{30}$$

Finally, the additional surface force along the outline of the cavern induced by the tunnel can be obtained approximately. On the other hand, the additional surface force induced by the cavern along the outline of the tunnel can be obtained through similar process.

3.3 The First Solution for the Cavern

With the action of the additional surface force, the analytic functions for the cavern in Z_2 half-plane are

$$\varphi_{21}(z_2)=\varphi_{21}(\omega_2(\zeta_2))=\varphi_{21}(\zeta_2)=\sum_{k=0}^{\infty}a_k^{21}\zeta_2^k+\sum_{k=1}^{\infty}b_k^{21}\zeta_2^{-k} \tag{31}$$

$$\psi_{21}(z_2)=\psi_{21}(\omega_2(\zeta_2))=\psi_{21}(\zeta_2)=\sum_{k=0}^{\infty}c_k^{21}\zeta_2^k+\sum_{k=1}^{\infty}d_k^{21}\zeta_2^{-k} \tag{32}$$

It should be noted that the analytic functions for the cavern in the first iteration contains only the series terms, excludes the logarithm term, because the resultant force of the additional

surface force is zero after integrating a whole circle around the cavern. In the second and subsequent iterations, the analytic functions for the tunnel and the cavern only contain the series terms for the same reason.

On the ground surface, the stress free condition is considered, and the boundary condition is expressed as follows

$$\varphi_{21}(\sigma)+\frac{\omega_2(\sigma)}{\omega_2'(\sigma)}\overline{\varphi_{21}'(\sigma)}+\overline{\psi_{21}(\sigma)}=0 \tag{33}$$

On the cavern boundary, the additional surface forces are applied, and the boundary condition is expressed as follows

$$\varphi_{21}(\alpha_2\sigma)+\frac{\omega_2(\alpha_2\sigma)}{\omega_2'(\alpha_2\sigma)}\overline{\varphi_{21}'(\alpha_2\sigma)}+\overline{\psi_{21}(\alpha_2\sigma)}=\sum_{k=-m}^{m}E_k\sigma^k+C_2 \tag{34}$$

With the conditions at the ground surface and the cavern boundary, all power coefficients in the analytic functions $\varphi_{21}(\zeta_2)$ and $\psi_{21}(\zeta_2)$ can be determined by the power series method in Section 3.1.

According to the principle of Schwarz alternating method, the calculation process of subsequent iterations is the same as that described in Section 3.1. The final analytic functions can be obtained by superposing the analytic functions of each iteration.

$$\begin{cases}\varphi_i(z_i)=\sum_{j=1}^{L}\varphi_{ij}(\xi_i)\\ \psi_i(z_i)=\sum_{j=1}^{L}\psi_{ij}(\xi_i)\end{cases} \tag{35}$$

where i = 1, 2 represent the tunnel and the cavern, respectively. L is the total numbers of iteration.

3.4 Formulas for Stresses and Displacements

In order to compute the ground stress and deformation conveniently, some coordinate systems are established as shown Fig. 5.

The *xoy* coordinate system coincides with $x_1o_1y_1$, and the coordinates in these coordinate systems satisfy the following relationships

$$r\cos\beta=x'=x=x_1=x_2+c \tag{36}$$

$$r\sin\beta=y'=y+h_1=y_1+h_1=y_2+h_1 \tag{37}$$

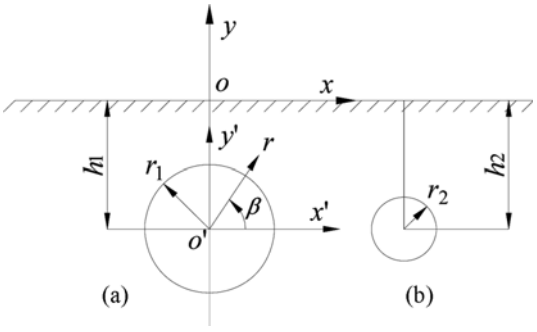

Fig. 5. Coordinate Systems: (a) Tunnel, (b) Cavern

The formulas for stresses of any point (*x*, *y*) in the *xoy* coordinate system are

$$\sigma_x^i+\sigma_y^i=2\left[\varphi_i'(z_i)+\overline{\varphi_i'(z_i)}\right] \tag{38}$$

$$\sigma_x^i-\sigma_y^i+2i\tau_{xy}^i=2\left[\overline{z_i}\varphi_i''(z_i)+\psi_i'(z_i)\right] \tag{39}$$

where i = 1, 2 represent the tunnel and the cavern, respectively.

Before excavation, stresses caused by gravity are determined by Eq. (5). The total stresses in the *xoy* coordinate system are

$$\begin{cases}\sigma_x=\sigma_x^0+\sigma_x^1+\sigma_x^2\\ \sigma_y=\sigma_y^0+\sigma_y^1+\sigma_y^2\\ \tau_{xy}=\tau_{xy}^0+\tau_{xy}^1+\tau_{xy}^2\end{cases} \tag{40}$$

According to the relations between the $x'o'y'$ system and the *xoy* system, the stresses of any point (*x*,*y*) in the $x'o'y'$ system can be determined. Then, the stresses in the $r\ \beta$ system can be determined

$$\begin{cases}\sigma_r=\frac{\sigma_x'+\sigma_y'}{2}+\frac{\sigma_x'-\sigma_y'}{2}\cos2\beta+\tau_{xy}'\sin2\beta\\ \sigma_\beta=\frac{\sigma_x'+\sigma_y'}{2}-\frac{\sigma_x'-\sigma_y'}{2}\cos2\beta-\tau_{xy}'\sin2\beta\\ \tau_{r\beta}=\frac{\sigma_y'-\sigma_x'}{2}\sin2\beta+\tau_{xy}'\cos2\beta\end{cases} \tag{41}$$

where σ_r, σ_β and $\tau_{r\beta}$ are radial stress, hoop stress and tangential stress, respectively.

The formula for displacements of any point (*x*, *y*) in the *xoy* system is

$$u_i+v_i=\frac{1}{2G}\left[\kappa\varphi_i(z_i)-z_i\overline{\varphi_i'(z_i)}-\overline{\psi_i(z_i)}\right] \tag{42}$$

where *u* represents the horizontal displacement and *v* represents the vertical displacement. *G* represents the shear modulus of the ground, here $G = E/[2(1+\mu)]$. The displacements induced by the tunnel and the cavern in the *xoy* system could be added up

$$\begin{cases}u=u_1+u_2\\ v=v_1+v_2\end{cases} \tag{43}$$

3.5 Accuracy for the Solution

The precision of the solution is affected by the number of the non-zero positive and negative powers contained in the two series, the approximation of the additional surface force and the total number of iterations.

Some coefficients are abandoned in solving boundary equations. As a result, the stress boundary cannot be satisfied perfectly, that is the solution is approximate. The number *N* of the non-zero positive and negative powers contained in the two series plays a crucial role on the solving accuracy. Theoretically, the solution

becomes more accurate with the increases of N. Taking the first iteration of the tunnel as an example, 360 points are taken equidistantly on the tunnel boundary. Then the radial stress for each point could be determined by Eq. (41). The value of N is determined by $|\sigma_r/(\gamma h_1)| < 0.1\%$ for each point in this paper.

The approximation of the additional surface force is determined by the value m of the approximation series contained in Eq. (24) and the value M of points taken equidistantly on the tunnel boundary. The additional surface force calculated by Eq. (23) and Eq. (24) are named real value and approximate value, respectively. For this research, if the maximum relative error between the approximate value and the real value for all points on the tunnel boundary is less than 0.1%, the accuracy is supposed to be adequate. Through the trial it is found that the accuracy requirement can be satisfied when the value of m and M are 50 and 360, respectively.

Theoretically, the solving precision gets accurate with iterations, which can only be carried out finitely in the practical calculation. When the maximum radial stress for all points on the tunnel boundary satisfies $|\sigma_r/\gamma h_1| < 0.1\%$ in the last iteration, the accuracy is considered to be adequate.

4. Validation and Results of the Analytical Model

The basic model is established with a cavern on the right side of the tunnel. The parameters of the basic model are assumed as follows: $E = 10$ MPa, $\mu = 0.33$, $\gamma = 20$ kN/m^3, $K_0 = 0.5$, $r_1 = 3$ m, $r_2 = 1$ m, $h_1 = h_2 = 15$ m, $c = 5$ m, $d = 5$ m. The rest models are obtained by varying only one parameter based on the basic model. The positions of the cavern are shown in Fig. 6.

4.1 Verification of the Analytical Solution for Basic Model

By the finite element software ABAQUS, a numerical model (FEM) corresponding to the basic model is established. The dimension of the model size is 100 m × 100 m. Horizontal constraints are imposed on the lateral sides and vertical constraints are imposed on the bottom. As shown in Fig. 1, the numerical calculation is divided into two steps. The FEM (a) (corresponding to model Fig. 1(a)) before tunnel excavation under gravity condition is calculated, and the node forces on the tunnel boundary are extracted. Then, the equal but opposite nodal forces are imposed on the tunnel boundary in the FEM (b) (corresponding to model Fig. 1(b)) for solving. The numerical result for stress on the tunnel boundary can be obtained by superposing the stresses of the two models. However, the displacements only contain the result from FEM (b).

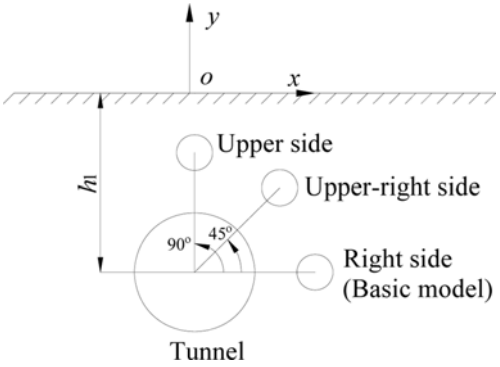

Fig. 6. Positions of the Caverns

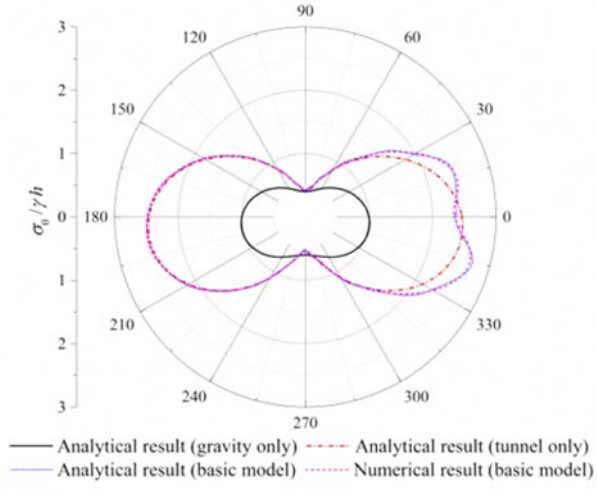

Fig. 7. Hoop Stresses on the Tunnel Boundary

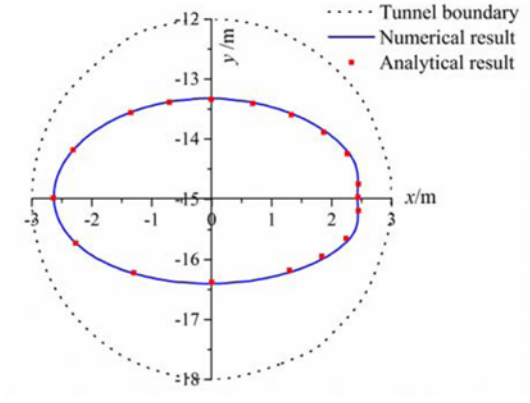

Fig. 8. Deformations on the Tunnel Boundary

In order to determine a_0 and c_0 in the two series, a fixed point should be selected. In this paper, the point P (shown in Fig. 2) is selected as the zero-displacement reference point, which is located below the tunnel with $3h_1$ from the surface. The displacements from the numerical result also subtract the displacement at point P. For the sake of clarity, the displacement shown in Fig. 8 is magnified 10 times. By comparing the analytical results with the numerical results, it is found that the maximum error of the hoop stress around the tunnel boundary is about 1.5% (shown in Fig. 7), and the maximum error of the deformation is about 2.6% (shown in Fig. 8). So the proposed analytical results agree well with those of the numerical method.

4.2 Hoop Stresses on the Tunnel Boundary

Figure 9 illustrates the effects of the center distance, the size and position of the cavern on the hoop stresses around the tunnel

boundary.

As shown in Figs. 9(a) and 9(b), when the cavern is on the right side of tunnel, the hoop stresses on the tunnel boundary are decreased in the range of 0°~5° and 355°~360°, and increased in the range of 5°~45° and 315°~355°. However, the effects induced by the cavern on the hoop stresses in the range of 45°~315° are not obvious. The minimum value of the hoop stresses is located near 0°, while the maximum values are located near 15° and 345°. Overall, the hoop stresses are symmetric about 0°-180°axis. The effects induced by the cavern are gradually decreased with the increase of the distance between the cavern center and the tunnel center (shown in Fig. 9(a)). As the cavern gets reduced,

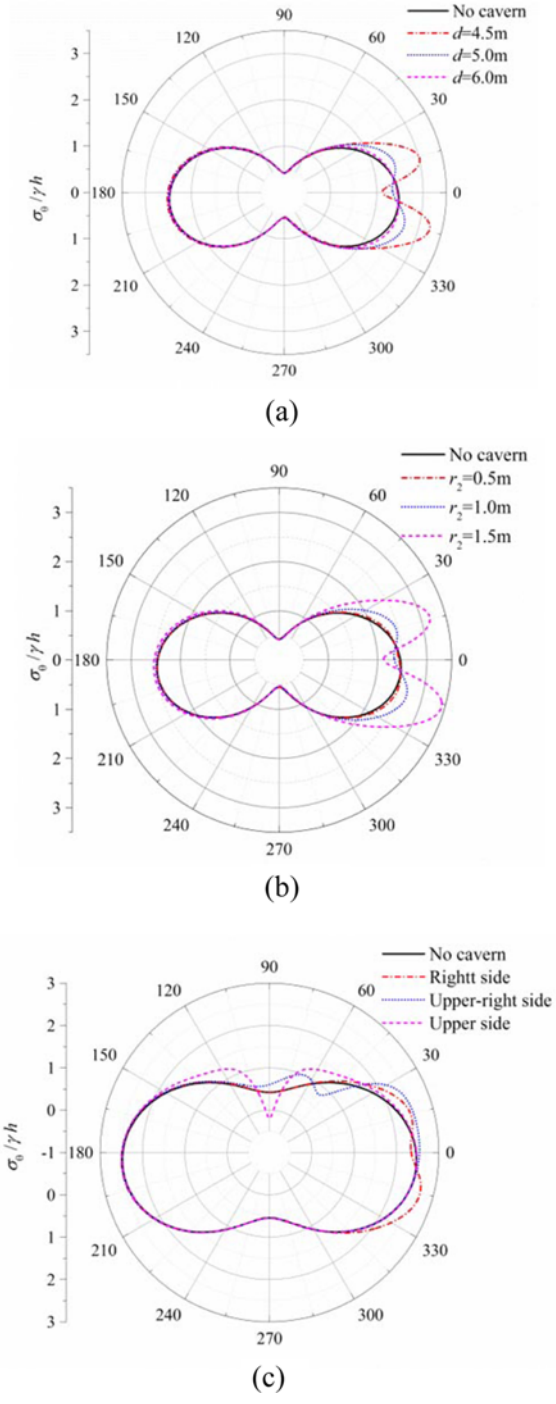

Fig. 9. Hoop Stresses on the Tunnel Boundary: (a) Effects of Center Distance d on Hoop Stresses, (b) Effects of the Cavern Size r_2 on Hoop Stresses, (c) Effects of the Cavern Position on Hoop Stresses

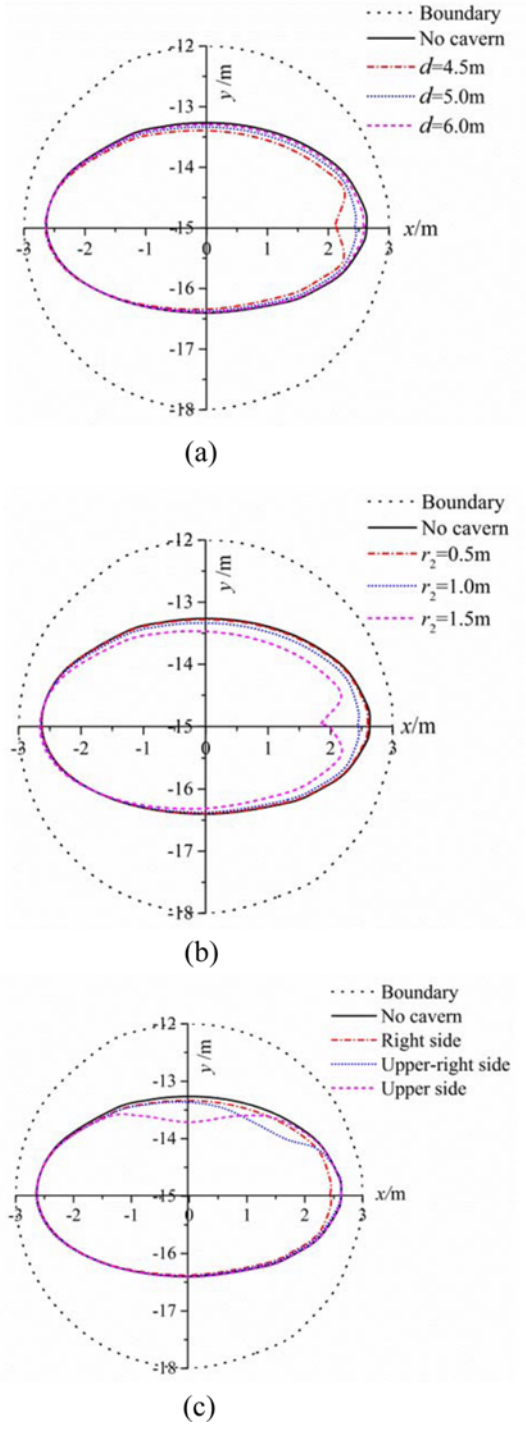

Fig. 10. Deformations on the Tunnel Boundary: (a) Effects of Center Distance d on Deformations, (b) Effects of the Cavern Size r_2 on Deformations, (c) Effects of the Cavern Position on Deformations

the effects are also decreased subsequently. When the radius of the cavern is less than 0.5 m, the variation of the hoop stress can be ignored (shown in Fig. 9(b)).

As shown in Fig. 9(c), when the cavern is located at the upper-right side of the tunnel, the hoop stresses on the tunnel boundary are decreased in the range of 40°~50° and increased in the range of 0°~40° and 50°~90°. The minimum value of the hoop stresses is located near 15°. While the cavern is located at the upper side of the tunnel, the hoop stresses would be decreased in the range 85°~95°, and increased in the range of 45°~85° and 95°~135°. What should be noted is that the hoop stress is transformed from pressure to tension at tunnel vault position in this case.

4.3 Deformations on the Tunnel Boundary

In Fig. 10, the effects of the center distance, the size and position of the cavern on the deformations around the tunnel boundary are shown. For the sake of clarity, the displacement is magnified 10 times in Fig. 10.

As seen in Figs. 10(a) and 10(b), the deformation on the right half of the tunnel is enlarged when the cavern is located at the right side of the tunnel. Among them, the peak value of the deformation happens near 0°. On the left half of the tunnel, the effects caused by the cavern are unremarkable. For example, the deformation at 180° is negligible. With the increase of the distance between the cavern center and the tunnel center, the effects caused by the cavern on the deformations are reduced gradually (shown in Fig. 10(a)). With the decrease of cavern size, the effects caused by the cavern are also reduced. While the cavern radius is less than 0.5 m, the effects can be ignored (shown in Fig. 10(b)).

In Fig. 10(c), the deformations are always enlarged on the cavern side no matter where the cavern is located, but the variation of the deformations is negligible on the other side. Among them, the maximum deformation is always located on the line between the tunnel center and the cavern center.

4.4 Surface Settlements

In Figs. 11, 12 and 13, it is assumed that the point on the ground surface x_1 = -45 m is fixed. The differential settlements are defined as the discrepancy between the surface subsidence with a cavern and the surface subsidence without a cavern.

As seen in Figs. 11 and 12, the surface settlements are increased above the cavern when the cavern is on the right side of the tunnel. Among them, the increment of surface settlement on the cavern's vertical axis is most significant. With the increase of the center distance and the decrease of the cavern size, the differential settlements are decreased gradually. It is not difficult to see that the curvature of the differential settlements closed to the tunnel side is larger than the other side, and the position of the maximum differential settlement is always near the cavern's vertical axis (shown in Figs. 11(b) and 12(b)).

As shown in Fig. 13, when the cavern is located at the upper-

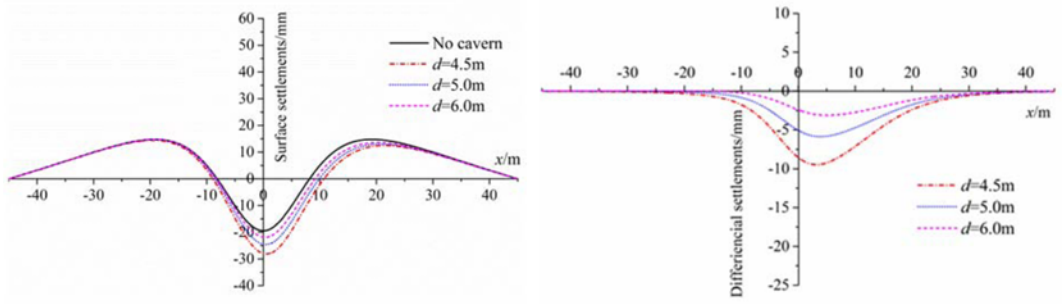

Fig. 11. Effects of Center Distance d on Surface Settlements: (a) Surface Settlements, (b) Differential Settlements

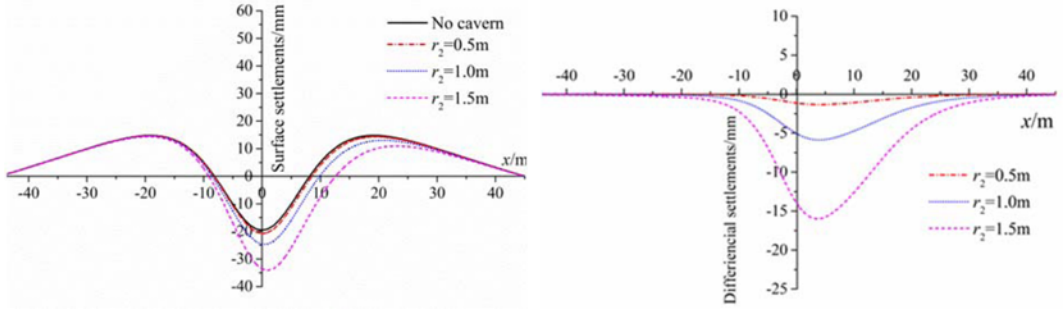

Fig. 12. Effects of the Cavern Size r_2 on Surface Settlements: (a) Surface Settlements, (b) Differential Settlements

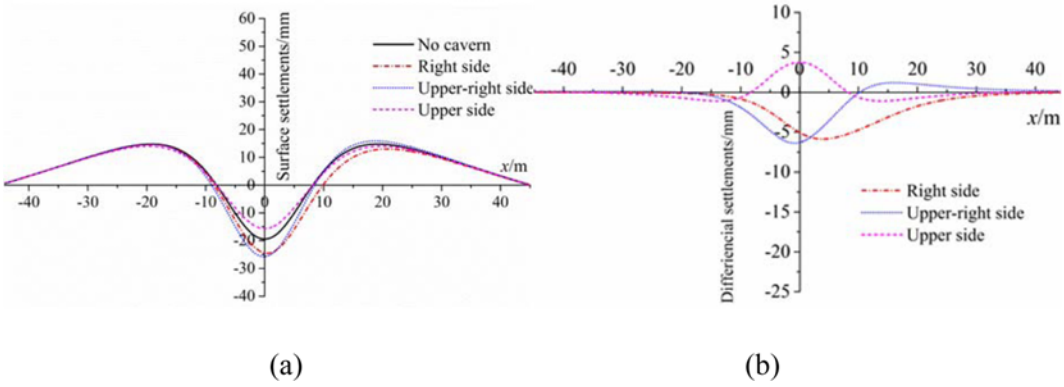

Fig. 13. Effects of Cavern Position on Surface Settlements: (a) Surface Settlements, (b) Differential Settlements

right side of the tunnel, the curve of differential settlement is moved to the tunnel side due to the decrease of center distance, and getting zero in far field. The surface settlements are increased when $x < 10$ m, but decreased when $x > 10$ m. What should be noted is that the maximum differential settlement is located at the left side of the y-axis instead of on the cavern's vertical axis. While the cavern is on the upper side of the tunnel, the differential settlements are symmetric about the y axis, and getting zero in far field. The surface settlements are decreased when $-9\text{ m} < x_1 < 9\text{ m}$, but increased slightly when $x_1 < -9$ m and $x_1 > 9$ m. This rule may be different from the actual phenomenon because the solution is an elastic solution and does not consider the plasticity of the soil. In the elastic solution, the cavern may absorb partial deformation and energy during the tunnel excavation, which results in the decrease of surface settlements. In fact, due to the plasticity of the soil, the tunnel excavation may lead to plastic deformations of the ground and result in the increase of surface subsidence. However, the elastic solution in this paper is still helpful for the case without serious plastic deformation.

5. Conclusions

A theoretical model is established for a shallow circular tunnel with a cavern in the stratum, in which the gravity condition and the interaction between the tunnel and the cavern are considered.

1. In the solving process, complex variable theory and Schwarz alternating method are applied. The iterative calculation is realized by a computer script. The accuracy of the solution is discussed from three aspects: the number of the two series, the approximation of additional surface force and the number of iterations.
2. In order to verify the analytical results, a numerical model corresponding to the basic analytical model is established. Then, the hoop stresses and the deformations on the tunnel boundary from analytical results and numerical results are compared, which indicates that the analytic solution agrees very well with the numerical solution.
3. The effects of the center distance, the size and position of the cavern on the ground stress and deformation are analyzed. The results show that the hoop stresses on the tunnel boundary are decreased in 0°~5° and increased in 5°~45° on both sides of the line between the tunnel center and the cavern center. The deformations on the tunnel boundary are enlarged near the cavern side with the maximum deformation on the line between the tunnel center and the cavern center. The surface settlements above the cavern are increased and the differential settlements get zero in far field when the cavern is located at the upper-right or right side of the tunnel, but the surface settlements will be decreased if the cavern is located at the upper side of the tunnel.

The soil mass is assumed as homogeneous elastic material, so the plasticity and viscosity of the ground are not considered.

The assumptions adopted in the solving process lead to some shortcomings of the solution in this paper, such as not considering the plasticity and viscosity of the ground, and not taking into account the longitudinal factors. Further research in these areas can be carried out in the future.

Acknowledgements

The research is supported by the Beijing Municipal Natural Science Foundation of China (Grant no.8172037) and the National Natural Science Foundation of Chia (Grant no: 51378002).

Notations

The following symbols are used in this paper:

$a_k^{ij}, b_k^{ij}, c_k^{ij}, d_k^{ij}$ = coefficients of the analytic functions, i is the identifier of the cavity, j is the number of iterations, k is identifier of the series

C_i = integration constant, i is the serial number of the cavity

c = distance between the origins of $x_1o_1y_1$ and $x_2o_2y_2$

d = distance between centers of the tunnel and the cavern

E = Young's modulus of ground

F_{lx}, F_{ly} = resultant force on tunnel boundary in x direction and y direction, respectively

f_{ij} = additional surface force, i is the identifier of the cavity, j is the number of iterations

G = shear modulus of ground
g_1, g_2 = real and imaginary part of f_{ij}, respectively
h_1, h_2 = center depth of the tunnel and the cavern, respectively
K_0 = lateral stress coefficient of ground
L = total numbers of iteration
l = direction cosine of the outward normal unit vector in x_1 direction on the tunnel boundary
M = number of points are taken equidistantly in the interval $(0, 2\pi)$
m = maximum number of the series of the approximation for the additional surface force
N = positive (negative) items contained in the two series
n = direction cosine of the outward normal unit vector in y_1 direction on the tunnel boundary
r_1, r_2 = radius of the tunnel and the cavern, respectively
r, β = polar coordinates
X_n, Y_n = surface force in x direction and y direction on the tunnel boundary, respectively
u_i, v_i = horizontal and the vertical displacement in xoy coordinates, i is the identifier of the cavity
α_i = radius of the inner circular for mapping plane, i is the identifier of the cavity
ω_i = conformal transformation function, i is the identifier of the cavity
κ = material constant related to Poisson's ratio
η_i = points on the cavity boundary on the mapping plane, i is the identifier of the cavity
φ_{ij}, ψ_{ij} = complex potential functions. i is the identifier of the cavity, j is the number of iterations
φ_i, ψ_i = final complex potential functions, i is the identifier of the cavity
$\varphi_0 \psi_0$ = single-valued analytic functions
γ = uniform weight of ground
μ = Poisson's ratio of ground
σ_x^0, σ_y^0, τ_{xy}^0 = stress of ground before tunnel excavation in xoy coordinates
σ_x^i, σ_y^i, τ_{xy}^i = stress of ground induced by cavity i in xoy coordinates, i is the serial number of the cavity
σ_x, σ_y, τ_{xy} = total stress of ground in xoy coordinates
σ'_x, σ'_y, τ'_{xy} = total stress of ground in $x'o'y'$ coordinates
σ_r, σ_β, $\tau_{r\beta}$ = total stress of ground in $r\beta$ coordinates

ORCID

Chengping Zhang https://orcid.org/0000-0001-6811-2971

References

Addenbrooke, T. I. and Potts, D. M. (2001). "Twin tunnel interaction: Surface and subsurface effects." *International Journal of Geomechanics*, Vol. 1, No. 2, pp. 249-271, DOI: 10.1061/(ASCE)1532.-3641(2001)1:2(249).

Augarde, C. E., Lyamin, A. V., and Sloan, S. W. (2003). "Prediction of undrained sinkhole collapse." *Journal of Geotechnical and Geoenvironmental Engineering*, Vol. 129, No. 3, pp. 197-205, DOI: 10.1061/(ASCE) 1090-0241(2003)129:3(197).

Bobet, A. (2001). "Analytical solutions for shallow tunnels in saturated ground." *Journal of Engineering Mechanics*, Vol. 127, No. 12, pp. 1258-1266, DOI: 10.1061/(asce)0733-9399(2001)127:12(1258).

Do, N. A., Dias, D., and Oreste, P. (2016). "3D numerical investigation of mechanized twin tunnels in soft ground-influence of lagging distance between two tunnel face." *Engineering Structures*, Vol. 109, pp. 117-125, DOI: 10.1016/j.engstruct.2015.11.053.

Fang, Q., Zhang, D. L., and Wong, L. N. Y. (2011). "Environmental risk management for a cross interchange subway station construction in China." *Tunnelling and Underground Space Technology*, Vol. 26, No. 6, pp. 750-763, DOI: 10.1016/j.tust.2011.05.003.

Fu, J. Y., Yang, J. S., Yan, L., and Abbas, S. M. (2015). "An analytical solution for deforming twin-parallel tunnels in an elastic half plane." *International Journal for Numerical and Analytical Methods in Geomechanics*, Vol. 39, No. 5, pp. 524-538, DOI: 10.1002/nag.2322.

Goodings, D. J. and Abdulla, W. A. (2002). "Stability charts for predicting sinkholes in weakly cemented sand over karst limestone." *Engineering Geology*, Vol. 65, Nos. 2-3, pp. 179-184, DOI: 10.1016/S0013-7952(01)00127- 2.

Lee, K. M. and Rowe, R. K. (1990). "Finite element modelling of the three-dimensional ground deformations due to tunnelling in soft cohesive soils: Part I - Methods of analysis." *Computers and Geotechnics*, Vol. 10, No. 2, pp. 87-109, DOI: 10.1016/0266-352X(90)90001-C.

Lee, K. M., Rowe, R. K., and Lo, K. Y. (1992). "Subsidence owing to tunneling. I. Estimating the gap parameter." *Canadian Geotechnical Journal*, Vol. 29, No. 6, pp. 929-940, DOI: 10.1139/t92-104.

Li, Q. Q., Zhang, D. L., and Fang, Q. (2014). "Analytic solution to initial damage of cavern strata by complex function method." *Chinese Journal of Geotechnical Engineering*, Vol. 36, No. 11, pp. 2110-2117, DOI: 10.11 779/CJGE201411018 (In Chinese).

Liu, X. R., Liu, Y. Q., Yang, Z. P., and He, C. M. (2017). "Numerical analysis on the mechanical performance of supporting structures and ground settlement characteristics in construction process of subway station built by pile-beam-arch method." *KSCE Journal of Civil Engineering*, Vol. 21, No. 5, pp. 1690-1705, DOI: 10.1007/s12205-016-0004-9.

Loganathan, N. and Poulos, H. G. (1998). "Analytical prediction for tunneling-induced ground movements in clays." *Journal of Geotechnical & Geoenvironmental Engineering*, Vol. 124, No. 9, pp. 846-856, DOI: 10.1 061/(ASCE)1090-0241(1998)124:9(846).

Lu, A. Z., Zeng, X. T., and Xu, Z. (2016). "Solution for a circular cavity in an elastic half plane under gravity and arbitrary lateral stress." *International Journal of Rock Mechanics & Mining Sciences*, Vol. 89, No. 8, pp. 34-42, DOI: 10.1016/j.ijrmms.2016.08.004.

Migliazza, M., Chiorboli, M., and Giani, G. P. (2009). "Comparison of analytical method, 3D finite element model with experimental subsidence measurements resulting from the extension of the Milan underground." *Computers and Geotechnics*, Vol. 36, Nos. 1-2, pp. 113-124, DOI: 10.1016/j.compgeo.2008.03.005.

Park, K. H. (2004). "Elastic solution for tunneling-induced ground movement in clay." *International Journal of Geomechanics*, Vol. 4, No. 1, pp. 310-318, DOI: 10.1061/(ASCE)1532-3641(2004)4:4(310).

Peck, R. B. (1969). "Deep excavations and tunneling in soft ground." *Proc. of the 7th Int. Conf. on Soil Mechanics and Foundation Engineering*, State of Art, Mexico City, Mexico, pp. 225-290.

Sagaseta, C. (1987). "Analysis of undrained soil deformation due to

ground loss." *Géotechnique*, Vol. 37, No. 3, pp. 301-320, DOI: 10.1680/geot.1987.37.3.301.

Strack, O. E. and Verruijt, A. (2002). "A complex variable solution for a deforming buoyant tunnel in a heavy elastic half-plane." *International Journal for Numerical and Analytical Methods in Geomechanics*, Vol. 26, No. 12, pp. 1235-1252, DOI: 10.1002/nag.246.

Verruijt, A. (1997). "A complex variable solution for a deforming circular tunnel in an elastic half-plane." *International Journal for Numerical and Analytical Methods in Geomechanics*, Vol. 21, No. 2, pp. 77-89, DOI: 10.1002/(sici)1096-9853(199702)21:2<77::aid-nag857>3.0.co;2-m.

Verruijt, A. (1998). "Deformations of an elastic half-plane with a circular cavity." *International Journal for Solids and Structures*, Vol. 35, No. 21, pp. 2795-2804, DOI: 10.1016/S0020-7683(97)00194-7.

Zhang, Z. G., Huang, M. S., Xi, X. G., and Yang, X. (2018). "Complex variable solutions for soil and liner deformation due to tunneling in clays." *International Journal of Geomechanics*, Vol. 18, No. 7, pp. 1-19, DOI: 10.1016/(asce)gm.1943-5622.0001197.

Zhang, L. Q., Yang, Z. F., and Lu, A. Z. (2000). "Analytical study on plane elastic problem of two random geometry tunnels." *Science in China (Series D)*, Vol. 30, No. 5, pp. 509-518, DOI: 10.3321/j.issn:1006-9267.2000.05.009 (In Chinese).

Zhang, Z. G., Zhang, M. X., Jiang, Y. J., Bai, Q. M., and Zhao, Q. H. (2017). "Analytical prediction for ground movements and liner internal forces induced by shallow tunnels considering non-uniform convergence pattern and ground-liner interaction mechanism." *Soils and Foundations*, Vol. 57, No. 2, pp. 211-226, DOI: 10.1016/j.sandf.2017.03.004.

Zhang, Z. G., Zhang, C. P., Jiang, K. M., Wang, Z. W., Jiang, Y. J., Zhao, Q. H., and Lu, M. H. (2019). "Analytical prediction for tunnel-soil-pile interaction mechanics based on Kerr foundation model." *KSCE Journal of Civil Engineering*, Vol. 23, No. 6, pp. 2756-2771, DOI: 10.1007/s12205-019-0791-x.

Zhang, C. P., Zhang, X., Li, H., and Zhang, D. L. (2016). "Model tests on failure laws of ground with voids induced by shallow tunneling." *Chinese Journal of Geotechnical Engineering*, Vol. 38, No. 2, pp. 263-270, DOI: 10.11 779/CJGE201602009 (In Chinese).

Zhou, S. W., Rabczuk, T., and Zhuang, X. Y. (2018). "Phase field modeling of quasi-static and dynamic crack propagation: COMSOL implementation and case studies." *Advances in Engineering Software*, Vol. 122, pp. 31-49, DOI: 10.1016/j.advengsoft:2018.03.012.

Zhou, S. W., Zhuang, X. Y., and Rabczuk, T. (2019). "Phase-field modeling of fluid-driven dynamic cracking in porous media." *Computer Methods in Applied Mechanics and Engineering*, Vol. 350, pp. 169-198, DOI: 10.1016/j.cma:2019.03.001.

Appendix 1. Expression of B_k

Let

$$T_1 = \frac{i\kappa\gamma r_1^2}{4(1+\kappa)}$$

$$T_2 = \frac{i\gamma r_1^2}{4(1+\kappa)\alpha_1}$$

$$T_3 = -\frac{iK\gamma a_1^2\left(1-\alpha_1^2\right)^2}{2}$$

$$T_4 = -\frac{2i\gamma a_1^2\alpha_1^3}{\alpha_1^2-1}$$

$$T_5 = \frac{i\gamma a_1^2\left(1+5\alpha_1^2+5\alpha_1^4+\alpha_1^6\right)}{2\left(\alpha_1^2-1\right)}$$

$$T_6 = -\frac{2i\gamma a_1^2(\alpha_1+\alpha_1^3+\alpha_1^5)}{\alpha_1^2-1}$$

$$T_7 = \frac{i\gamma a_1^2(\alpha_1^2+\alpha_1^4)}{\alpha_1^2-1}$$

$$R_k = \frac{\alpha_1^{k+2}}{\left(\alpha_1^2-1\right)^2},\ (k\geq 0)$$

$$S_k = \frac{\left[k\left(1-\alpha_1^2\right)+2\alpha_1^2-1\right]\alpha_1^{k-2}}{\left(\alpha_1^2-1\right)^2},\ (k\geq 1)$$

Then the coefficients B_k can be expressed as follows:

$$B_0 = T_1\left(1-\alpha_1^2\right)-T_2\alpha_1+T_3S_2+T_4S_3+T_5S_2+T_6S_1+T_7R_0$$

$$B_1 = T_1\alpha_1+T_2\left(1-\alpha_1^2\right)+T_3S_1+T_4S_2+T_5S_1+T_6R_0+T_7R_1$$

$$B_2 = T_2\alpha_1+T_3R_0+T_4S_1+T_5R_0+T_6R_1+T_7R_2$$

$$B_k = T_3R_{k-2}+T_4R_{k-3}+T_5R_{k-2}+T_6R_{k-1}+T_7R_k,\ (k\geq 3)$$

$$B_{-1} = -T_1\alpha_1+T_3S_3+T_4S_4+T_5S_3+T_6S_2+T_7S_1$$

$$B_{-k} = T_3S_{k+2}+T_4S_{k+3}+T_5S_{k+2}+T_6S_{k+1}+T_7S_k,\ (k\geq 2)$$